Spiral Instabilities in a Reaction−Diffusion System

Lu Qun Zhou and Qi Ouyang*

Department of Physics, Mesoscopic Physics Laboratory, Peking University, Beijing 100871, P. R. China

Received: July 7, 2000; In Final Form: October 24, 2000

We report our experimental study on spiral instabilities in an open spatial reactor using the Belousov−Zhabotinsky (BZ) reaction. A phase diagram showing different regimes of spiral dynamics is built. Two instabilities are identified in the phase diagram: the Doppler instability and the long wavelength instability. Both instabilities lead the system to a state of spatiotemporal chaos or chemical turbulence. In the regime of the Doppler instability, spiral waves break near the spiral core, when a Hopf bifurcation contributes to the spiral core, making the latter meander; in the regime of the long wavelength instability, a sustained long-wavelength modulational spiral appears and is stable in a range of control parameters. At the same time, the trajectory of the spiral tip changes from circular to epicycloid, which is very similar to a meandering spiral. The essential difference to distinguish meandering spirals from those with long wavelength modulations is that the convective velocity of the former is zero, while the latter is nonzero. Beyond that range of the control parameter, spiral waves break and the system undergoes a transition to chemical turbulence.

Introduction

In recent years, study of spiral dynamics has attracted a great deal of attention from researchers in different fields, such as nonlinear physics, mathematics, physical chemistry, biology, and cardiology. There are several reasons for these attractions. From a practical point of view, it is believed that a spiral performs an essential role in cardiac arrhythmia and fibrillation,[1−3] so understanding spiral dynamics has a promising application potential in cardiology. From theoretical point of view, the dynamics of spiral waves is dominated by its tip's movement, which can be considered as a topological defect. Study of spiral behavior will give hints about the defect dynamics. Moreover, transitions from ordered spiral waves to defect-mediated turbulence have been well-studied in theory[4−8] and observed both in experiments[9−12] and numerical simulation.[13−16] This is one of the most promising routes to investigate spatiotemporal chaos, which are poorly understood at present.

The dynamical behavior of spiral waves in an excitable medium is governed by a dispersion relation that relates the speed to the period of the traveling waves. In general, the speed depends on how rapidly a local system recovers its quiescent state after being excited; hence, it is an increasing function of the period of waves.[17] There exists a minimum period below which the system cannot recover to its excitable state and traveling waves cease to exist.[17,18] Usually, the period of regular spiral waves is larger than the minimum period; thus, spiral waves are stable. On the other hand, stable single spirals are two- or three-dimensional structures. Their rotating frequency and speed are influenced by the wave front curvature, so they obey the constitutive relation.[17] It is the two relations that determine the dynamical behavior of spiral waves, that is, the relations between their speed, wavenumber, and frequency.

A spiral head (or tip) is considered as a wave source, a wave being sent out after the head moves one circle. Therefore the spiral head movement includes abundant information about the behavior of a spiral, and its dynamics is possibly the key to interpret the behavior of spiral waves. For example, the meandering phenomenon of a spiral can be explained by a Hopf bifurcation contributing to the spiral tip.[19] Several models have been proposed to study the relation between the wavelength of a spiral and its core size, in turn the relation between the speed of the wave front and that of the spiral tip, such as the one describing the spiral movement by analogy with the combustion of grass,[20] or a more complete analysis of excitable reaction-diffusion media.[21]

Recently, two important spiral instabilities were experimentally found in a quasi-two-dimensional spatial open reactor using the Belousov−Zhabotinsky (BZ) reaction, the Doppler instability[12] and the long wavelength instability,[9,22] which result in spiral wave breakup and chemical turbulence. The cause for the former is a Hopf bifurcation contributing to the spiral core, which creates the spiral meandering. Tracing the movement of the spiral tip, one can find that the trajectory of the tip changes from a single circle to a flower with the control parameter varied. Due to the Doppler effect, with sufficiently large meandering, defects can be generated when two adjacent wave fronts near the core are too close, so the local wavelength is beyond the critical value allowed by the dispersion relation. This kind of instability possibly accounts for cardiac fibrillation.[23] When the latter, long-wavelength instability takes place, apparent spatially modulated waves emerge, so the distance between successive wave fronts (the local wavelength) varies spatially. As the amplitude of modulation increases with control parameters, spiral waves break.

In this paper, after introducing the experimental setup in the Experimental Section, we present our systematic studies of dynamical behaviors of spiral waves and spiral instabilities. A phase diagram with sulfuric acid and malonic acid as control parameters is built, and the lines of onsets for the Doppler instability and the long wavelength instability are identified. Both instabilities lead to chemical turbulence, but they show different phenomena and have different mechanisms. The following two sections describe the dynamical behavior of these two instabilities, respectively. At the end of the paper, we give some discussions.

* Correpondent author. E-mail: qi@mail.phy.pku.edu.cn.

10.1021/jp002430h CCC: $20.00
Published on Web 12/15/2000

Experimental Section

Our experiments are conducted in a spatial open reactor[24] using the ferroin ($Fe(phen)_3^{2+}$) catalyzed BZ reaction. The heart of the reactor is a thin porous glass disk (Vycor glass, Corning), 0.4 mm thick and 19.0 mm in diameter, which has 25% void space and 100 Å average pore size. The porous glass is used to prevent convection in the reaction medium. Each surface of the disk is in contact with a compartment where the reactant concentrations are kept homogeneous and constant by highly precise pumps and magnetic stirrers. The chemicals are fed asymmetrically: malonic acid and potassium bromide are fed on side A, sulfuric acid and ferroin are fed on side B, sodium bromate is fed on both sides, so that side A is kept fixed in a reduced state and side B in an oxidized state. Both sides are kept from oscillating. The chemicals diffuse into the porous glass, where the BZ reaction occurs and patterns form. Because multiple chemical gradients exist across the reaction medium, our system is in fact quasi-two-dimensional. However, previous studies[25,26] show that if the boundary conditions are uniform, the quasi-two-dimensional system with gradients in the third dimension (like our experimental setup) behaves qualitatively like a two-dimensional system.

In our experiments, although we use magnetic stirrers to mix reactant solutions in the compartments, we cannot guarantee that the boundary conditions of the reaction medium are perfectly uniform. However, after estimating the magnitude of perturbations that diffuses from the surfaces to the middle of the disk, we find that a perturbation at the boundaries has very little effect in the patterned layer. Our line of reasoning is the following: Suppose the perturbation to a homogeneous steady state is an oscillation with frequency ω, i.e., $c(x,t) = A \exp(-i\omega t)$, where x points to the transverse direction and $\omega \sim 1$ s. Consider the simplest diffusion equation

$$\frac{\partial c(x,t)}{\partial t} = D_\perp \frac{\partial^2 c(x,t)}{\partial x^2}$$

where $D_\perp$ is the transverse diffusion constant across the porous glass, which is measured as $D_\perp \approx 7 \times 10^{-7}$ cm^2/s,[27] and then we can get the asymptotical distribution of the perturbation:

$$c(x,t) = A \exp\left(-\sqrt{\frac{\omega}{2D_\perp}}x\right) \exp\left[i\left(\sqrt{\frac{\omega}{2D_\perp}}x - \omega t\right)\right]$$

The thickness of the porous glass is $d \approx 0.04$ cm. Suppose the patterned layer is in the middle of the reaction medium, then the perturbation will decay exponentially to $\exp(-17)$, about 10^{-8} smaller than that in the boundaries. Such a small perturbation has little impact on the behavior of a spiral inside the porous glass. However, if a pattern is formed *not* in the middle of the disk but near the surface, this perturbation can strongly affect the spiral locally. From our observation, this case occurs under the conditions of higher concentration of malonic acid ([MA] > 1.5 M), which is far beyond our experimental conditions.

In the experiment, a helium−neon laser (1 mW, $\lambda = 633$ nm) is used to generate and guide spirals.[28] When a spiral is guided to the boundary of reaction medium, it is absorbed and disappeared. Thus initial conditions can be chosen such that only one spiral resides in the middle of the system. Once a spiral is prepared, it is studied by increasing or decreasing one of the chemical concentrations in a stepwise fashion while the others are fixed. Enough time is allowed between changes so that the system can relax to its new asymptotic state. The typical waiting time is about 1 h. The reactor is illuminated by a blue light source (about 550 nm). Images of the patterns are taken by a charge coupled device (CCD) camera and then digitized and stored in a computer for later processing.

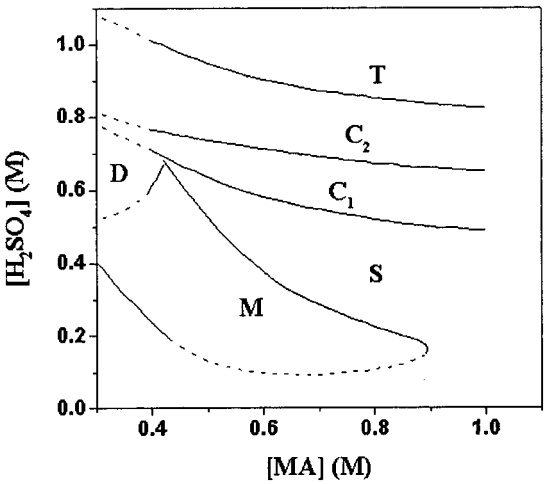

Figure 1. The phase diagram studied in our experiments with [MA] and $[H_2SO_4]$ as the control parameters. The solid lines indicate the onsets of different instabilities. The dashed lines are the extrapolation of the solid lines. The dotted line separates two types of modulational spirals (see text).

Phase Diagram

A previous study[29] shows that the dynamics of spiral waves is most sensitive to three control parameters: the concentrations of sulfuric acid ($[H_2SO_4]$), malonic acid ([MA]), and sodium bromate ($[NaBrO_3]$). At low $[NaBrO_3]$, we find the phenomena that we are interested in happening at high $[H_2SO_4]$ (>1 M). Such a high concentration of H_2SO_4 makes patterns unclear and can erode the chemical pumps, so we fix $[NaBrO_3] = 0.6$ M and choose $[H_2SO_4]$ and [MA] as control parameters. Other reactant concentrations of the BZ reaction are kept fixed: [KBr] = 0.03 M, [ferroin] = 0.15 mM. The experimental temperature is 25 ± 0.5 °C.

Figure 1 gives a slice of the phase diagram using [MA] and $[H_2SO_4]$ as control parameters. About 80 different points are studied and categorized. The phase diagram can be divided into several domains, and each is labeled according to the observed patterns: simply rotating spiral (S), meandering spiral (M), chemical turbulence due to the Doppler instability (D), convectively unstable spiral (C), and chemical turbulence due to the long wavelength instability (T). The solid lines give the onsets for several types of instabilities of spirals. Figure 2 shows examples of the ordered or disordered patterns in different regimes.

The S−M boundary in the phase diagram defines a transition from simple spirals to meandering spirals. At the onset, the spiral tip undergoes a Hopf bifurcation.[28] As a result, the trajectory of the tip changes from a simple circle to an epicycloid or a hypocycloid, and the local behavior of the spiral waves changes from periodic to quasi-periodic. In the meandering state, due to the Doppler effect, the tip of a spiral emits waves that are compressed in front of the tip and dilated behind the tip. Thus the local wavelength of spiral waves is no longer constant but changes periodically between a maximum and a minimum value. The ensemble of local maximum wavelength forms a super-spiral, as can be observed in Figure 2b. If one continues to decrease [MA] or to increase $[H_2SO_4]$ to cross the M−D boundary (see Figure 1), the Doppler instability will take place

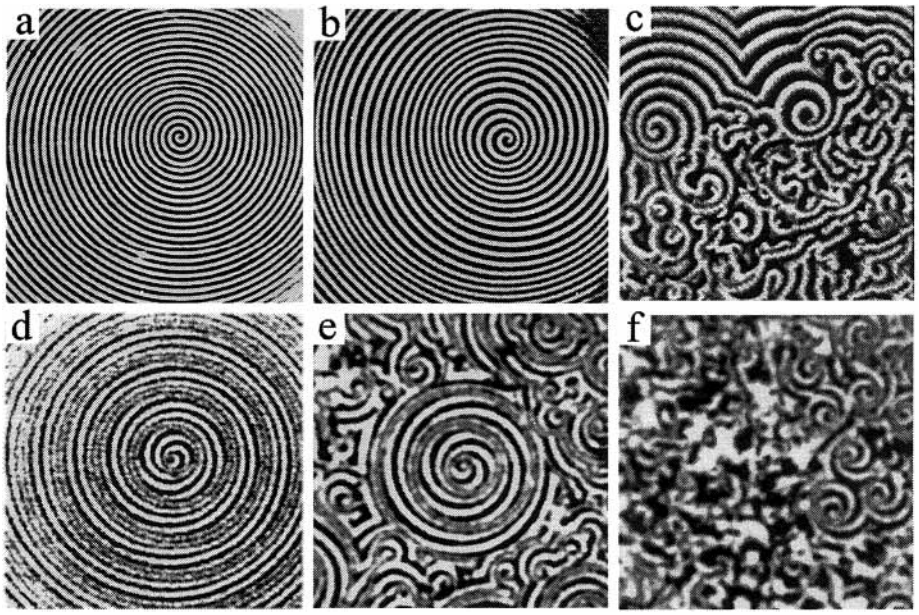

Figure 2. Examples of different patterns observed in the experiment: (a) a single spiral (S), (b) a meandering spiral (M), (c) a state of chemical turbulence due to the Doppler instability (D), (d) a modulational spiral due to the long wavelength instability (C_1), (e) the coexistence of a modulational spiral and chemical turbulence (C_2), (f) a state of chemical turbulence due to the long wavelength instability (T).

and defects are perpetually generated near the spiral heads, until chemical turbulence occupies the whole reaction medium. An example of this turbulent state is shown in Figure 2c. We will describe this phenomenon in detail in the next section.

The C regimes in the phase diagram represent regions where spiral waves undergo a long wavelength instability that has a convective nature (see the note[30] in the references). Before the onset, one observes a stable simple rotating spiral (Figure 2a). At the onset of the instability (S−C boundary in Figure 1), a long-wavelength modulated spiral appears upon the carrier waves, as shown in Figure 2d. This modulation spiral seems stable within our finite size of reaction medium. Beyond the onset, defects can be generated far away from the spiral center. However, due to the convective nature of the instability,[31] stable modulated waves can exist in a finite size, surrounded by a defect sea; see Figure 2e. With the increase of $[H_2SO_4]$, the stable modulated waves are encroached upon by a sea of defects, till it fully disappears when the control parameter crosses the C−T boundary in the phase diagram. As a result, the chemical turbulence in the whole reaction medium forms; see Figure 2f. The middle dotted line in the C regimes separates two parts, C_1 and C_2, which respectively represents two types of dynamical behaviors of the modulation waves. In one type, the modulation period decreases with the control parameter; in other type, it increases with the control parameter. One example is given in Figure 3, which is made by fixing [MA] (0.8 M) and varying $[H_2SO_4]$. In Figure 3a, the descent rates of the carrier waves' periods (T_c) as a function of $[H_2SO_4]$ have different values, −7.7 and −2.7 s M^{-1}, respectively; in Figure 3b, one observes a turning point of the modulation period (T_m) as a function of the control parameter.

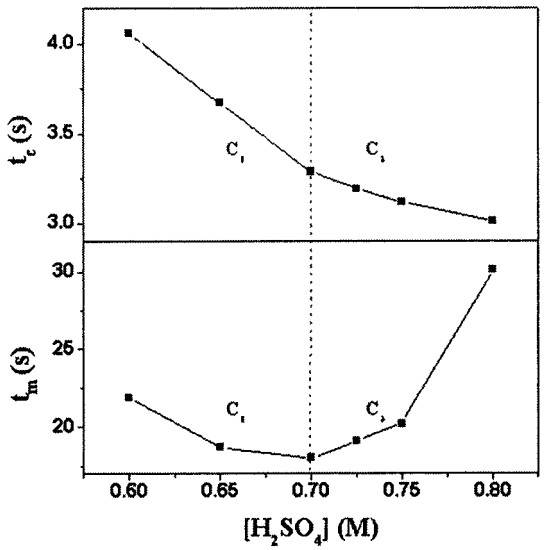

Figure 3. Two types of dynamical behaviors for the long wavelength instability. The dash line is at $[H_2SO_4] = 0.7$ M.

Doppler Instability

When [MA] is selected to be 0.4 M, the Doppler instability occurs as $[H_2SO_4]$ is increased to pass a critical value (about 0.6 M); hence, the system undergoes a transition from a meandering spiral to a state of defect-mediated turbulence or chemical turbulence. Figure 4 illustrates the development of this instability. At the beginning, only one spiral tip exists in the whole reaction medium, and its movement follows a epicycloid path (see Figure 4a). When the spiral tip meanders too close to its adjacent wave, the region near the tip touches and breaks the wave, generating a couple of defects, as shown in Figure 4b. These defects tend to meander away from one another and form rotating rotors (Figure 4c). As they do, the same process happens again. As time elapses, the number of the defects grows (Figure 4d−f), and the area of the disorder becomes wider until spiral defects saturate the whole system. We thus observe the spiral turbulence.

The instability leading to the spiral turbulence is caused by the Doppler effect on the spiral waves,[12] which is induced by a Hopf bifurcation contributing to the spiral tip and making it meander. As stated in the previous section, the Doppler effect makes a periodic variation of the local wavelength of the spiral waves. As the amplitude of meandering increases with the increase of control parameter ($[H_2SO_4]$ in this experiment), the minimum and the maximum local wavelength diverge; the

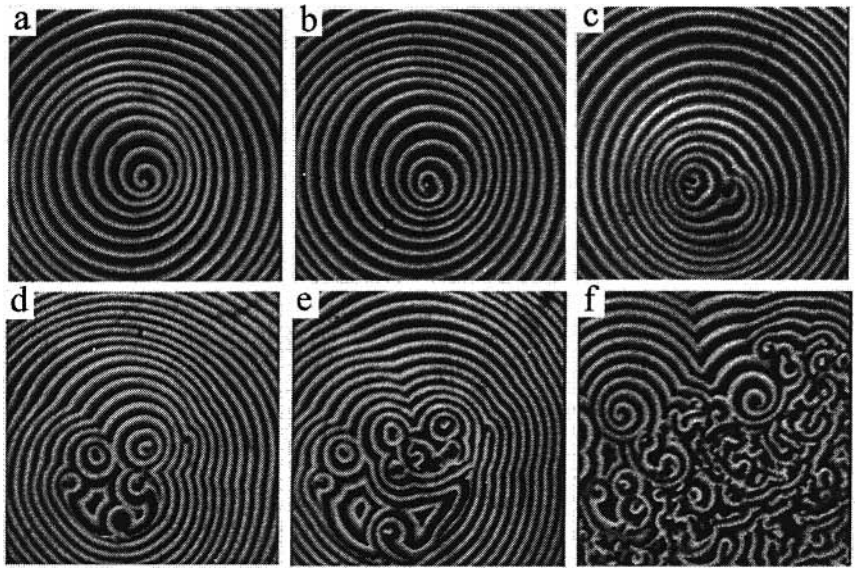

Figure 4. Development of chemical turbulence due to the Doppler instability.

minimum local wavelength becomes smaller, and the maximum is larger. As the control parameter crosses a critical value, the minimum local wavelength becomes lower than the minimum wavelength defined by the dispersion relation. Under this circumstance, a local spiral wave will change from stable to unstable and break into defects. Because of the dispersion relation, the difference of the minimum and the maximum wavelength will decrease as the spiral waves travel outward, so the most vulnerable region in a spiral is the area near the spiral tip. That is why the breaking point always occurs near the spiral core.

To summarize, the spiral breaking process for the Doppler instability is as follows: As the spiral tip moves toward its adjacent wave, making the local wavelength beyond the dispersion relation because of sufficiently large meandering,[13] it breaks the wave and generates a pair of defects. The newly generated defects drift apart and self-organize into new spiral rotors, which meander in the same way as their mother. Once it is formed, it has the chance to generate new defects. Repeatedly, daughter spirals give birth to granddaughter spirals, so that more and more defects emerge until the system is saturated with spiral defects. At last we observe a state of chemical turbulence.

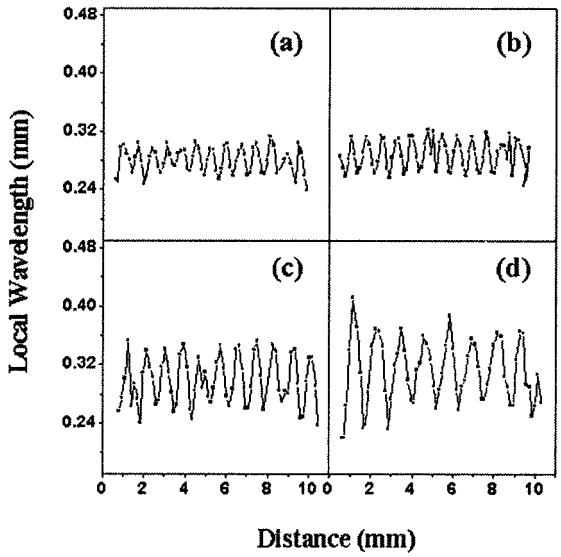

Figure 5. Local wavelengths of the modulational spiral waves for different [H_2SO_4] when [MA] = 0.8: (a) 0.6 M, (b) 0.65 M, (c) 0.7 M, and (d) 0.75 M. The origins are set at the points of the centers of the spiral waves, and squares correspond to the minimum or maximum amplitudes of the modulational spiral waves in one radial direction.

Long Wavelength Instability

Different from the Doppler instability, which leads to defects generated near the tip of a spiral, long wavelength instability creates defects appearing far away from the tip of spiral waves. In this section, we give some quantitative properties of this instability.

After the long wavelength instability occurs, apparent spatially modulated waves emerge so that the distance between successive wave fronts (the local wavelength) varies spatially, as shown in Figure 2d. The wavelength ratio of modulational and carrier waves is about 5, thus the instability is a long wavelength type. Figure 5 shows the variation of the local wavelengths. In the figure, the origins are set at the point of the spiral tip, and each point (solid square) corresponds to the local minimum or maximum amplitudes of the modulational spiral waves in the radial direction. One observes that the local wavelengths show periodic variation; both the average amplitude and the wavelength of phase modulation increase with the increase of [H_2SO_4], which means that the modulation becomes more obvious. Notice that the amplitudes of phase modulations are almost constant with the distance. Thus the perturbations to carrier spiral waves are saturated, and stable long-wavelength modulated spiral waves exist in our system.

The local wavelengths of a meandering spiral also periodically vary with the distance from the center of the waves, as shown in Figure 2b. However, there exists one qualitative difference between meandering spiral waves and modulational waves due to the long wavelength instability. If we follow one wave front with the speed of the carrier waves, for meandering spiral waves its local wavelength is almost constant with time, while for the long wavelength instability the local wavelength varies, which means that the modulation waves have a relative velocity (named convective velocity) v_g to the carrier waves. In our experiments, the direction of the convective velocity points to the center of the spiral waves. Table 1 gives the absolute values of the velocities for different [H_2SO_4]. It shows an increasing tendency with the increase of the parameter. Thus, the convective velocity

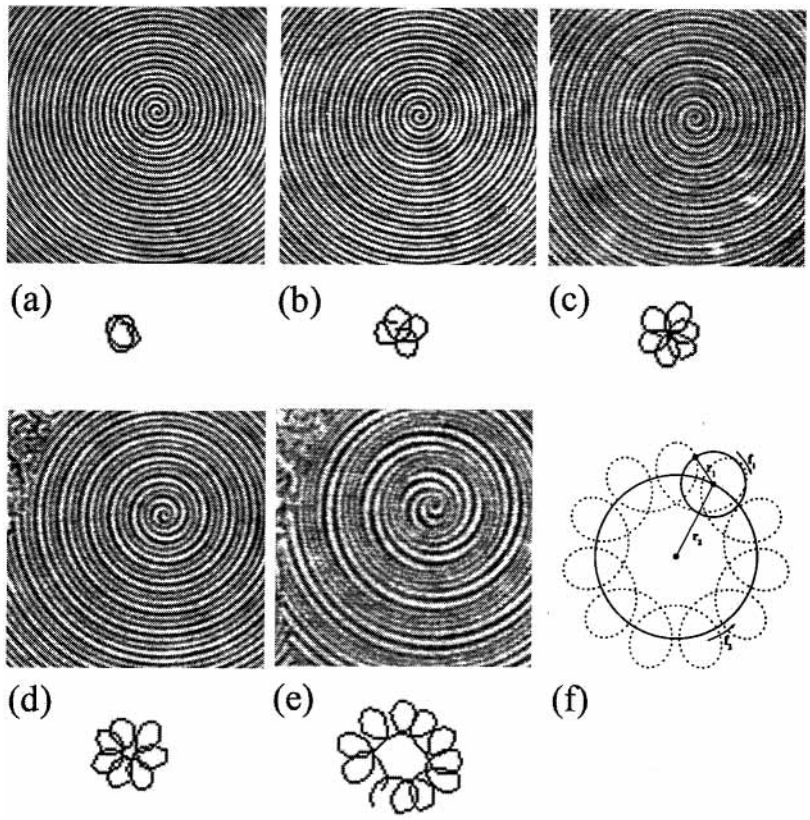

Figure 6. Modulational spirals and the trajectories of their tip's movements for different $[H_2SO_4]$ when [MA] = 0.8 M: (a) 0.6 M, (b) 0.65 M, (c) 0.7 M, (d) 0.725 M, and (e) 0.8 M. Each trajectory is arranged below the corresponding image (11×11 mm^2 in size) of the modulational spiral. (f) The typical epicycloid motion.

TABLE 1: Convective Velocity (v_g) Varies with $[H_2SO_4]$

$[H_2SO_4]$ (M)	0.6	0.65	0.7	0.725	0.8
v_g (mm/s)	1.42	1.43	1.49	1.57	1.78

v_g is an efficient order parameter to distinguish a meandering spiral from a modulation spiral in the case of the long wavelength instability.

The movement of a molulational spiral tip induced by the long wavelength instability is similar to that of a meandering spiral. Thus we trace this movement on amplified images and get flowerlike trajectories just as those appearing in the meandering spiral.[28] These flowers are plotted below images of modulational spirals in Figure 6a−e. Figure 6a shows a spiral and its tip trajectory near the onset of the long wavelength instability ($[H_2SO_4]$ = 0.6 M). As $[H_2SO_4]$ is increased, both the number of petals and the size of the flower are increased. One can see that all of them follow epicycloid motions with outward petals, as illustrated in Figure 6f, where the primary circle (radius r_1) orbits the secondary circle (radius r_2) with a rotational frequency f_2 in one direction and spins about its center with a spin frequency f_1 in the opposite direction. These two frequencies, f_1 and f_2, correspond, respectively, to ω_1 and $|\omega_1 - \omega_2|$ in the normal form analysis of Barkley[19] on the meandering spirals, where ω_1 is the primary frequency of a spiral and ω_2 is the frequency of spiral modulation in the rotating frame. Here we set $f_1 = \omega_1/2\pi$, and because of the epicycloid motions, one can get $\omega_2 > \omega_1$, then $f_2 = (\omega_2 - \omega_1)/2\pi$.

We determine f_1 by measuring the average frequency of spiral waves far from the spiral center and obtain f_2 from the relation $f_1/f_2 = n$, where n is the number of the petals of the flowers. The values of the primary frequency f_1 (or ω_1) are considered to be precise. But it is difficult to read the precise number of the petals n from the flowers; thus, we only give the approximate integers, respectively 3, 4, 6, 7, and 11. Therefore, we can approximately obtain the frequencies f_2 and ω_2 for different $[H_2SO_4]$. Notice that, due to the convective velocity v_g (see Table 1), the frequency f_2 is different from that measured in Figure 3b. We plot the spiral modulation frequency ω_2 for the long wavelength instability in Figure 7. We find that there also exist two types of dynamical behaviors of the modulational spiral waves, separated by $[H_2SO_4]$ = 0.7 M, which coincides with that shown in Figure 3. In the C_1 region ($[H_2SO_4] < 0.7$), the modulation period decreases with the increase of $[H_2SO_4]$; the tendency is the same as in Figure 3. However, in the C_2 region ($[H_2SO_4] > 0.7$ M), the two figures show different trends: the

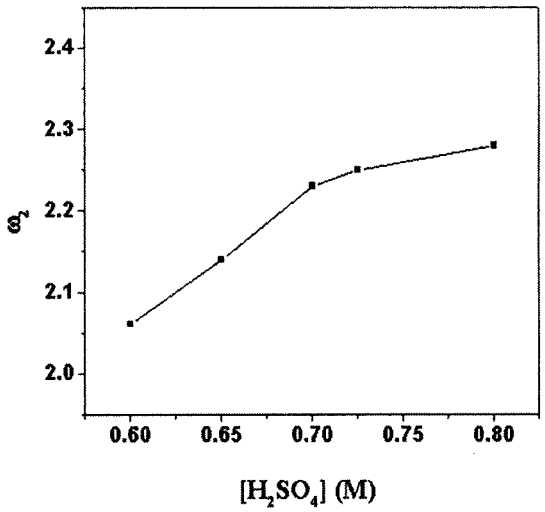

Figure 7. Frequency of spiral modulation ω_2 as a function of $[H_2SO_4]$.

period in Figure 3 becomes larger with the increase of [H_2SO_4], while the period in Figure 7 decreases a little.

If one increases [H_2SO_4] in the C_2 region, defects are continuously generated. The spiral breakup occurs far away from the center, and there exists a disk of ordered spiral pattern where turbulence cannot invade, as shown in Figure 2d. The system is thus separated into two different regimes: ordered spiral waves inside the disk and chemical turbulence outside of the disk. The size of the laminar disk decreases with the increase of the control parameter. When [H_2SO_4] is above the C−T boundary in the phase diagram (see Figure 1), the turbulence state will invade the whole space, which is the case of absolute instability.

Discussion

Two instabilities are observed in our experiments, the Doppler instability and the long wavelength instability. The mechanism of the former is clear and can be qualitatively compared with numerical simulations,[12] while the mechanism and the behavior of the latter need more discussion.

Single spiral waves far away from the spiral tip can be considered as planar wave trains in an oscillatory system. Near the onset of a Hopf bifurcation, the system's variable as a function of time t can be written: $c = c_0 + A\exp(i\omega_c t) + \text{c.c.}$ In a ferroin-catalyzed BZ reaction, c corresponds to the concentration of ferroin; ω_c is the Hopf frequency; and A is the complex amplitude of oscillations, which obeys the complex Ginzburg−Laudau equation (CGLE) in one dimension:

$$\tau_0 \frac{\partial A}{\partial t} = \mu A + (g_1 + ig_2)\frac{\partial^2 A}{\partial x^2} - \xi_0^{\,2}(d_1 + \mathrm{i}d_2)|A|^2 A \quad (1)$$

where τ_0 and ξ_0 are respectively the characteristic time and the correlation length of the system. g_1, g_2, d_1, and d_2 are related to the diffusion coefficients and ensemble of reaction kinetics. Using τ_0 and ξ_0 as time and length units, after rescaling we have

$$\frac{\partial A}{\partial t} A + (1 + \mathrm{i}\alpha)\frac{\partial^2 A}{\partial x^2} - (1 + \mathrm{i}\beta)|A|^2 A \quad (2)$$

where $\alpha = d_2/d_1$ and $\beta = g_2/g_1$ are control parameters. Equation 2 has traveling plane wave solutions $A_0 = F\exp[\mathrm{i}(qx - \omega_t)]$, where $F = 1 - q^2$ and $\omega = \alpha q + \beta(1 - q^2)$. They exist for $q^2 < 1$. To study the linear stability of the traveling waves, we consider perturbation of the form

$$A(x,t) = F[1 + a(x,t)]\exp\{1[qx - \omega t + \phi(x,t)]\}$$

where $a(x,t)$ and $\phi(x,t)$ represent respectively the perturbations to amplitude and phase of the traveling waves. Using the linear stability analysis, we seek solutions of the form $a_0\exp(\sigma t + \mathrm{i}px)$ and $\phi_0\exp(\sigma t + \mathrm{i}px)$ and look for the dispersion relation $\sigma(p)$. Near the onset there is a long wavelength ($p \sim 0$) critical mode ($\sigma(p) \sim 0$), which becomes a pure phase mode for $p \sim 0$. It is characterized by the following dispersion relation

$$\sigma = i\upsilon_g p - D_{|}p^2 + O(p^3) \quad (3)$$

where

$$\upsilon_g = 2(\beta - \alpha)q$$

$$D_{|} = 1 + \alpha\beta - \frac{2q^2(1 + \beta^2)}{1 - q^2}$$

When $D_{||} < 0$, the so-called Eckhaus instability occurs.[32,33] It is the long wavelength instability, and because of a nonzero υ_g, it has a convective nature.[30] Although the linear analysis shows the unstable mode $p \to 0$, the selected modulational wavelength by the nonlinear effect has a finite value for a system of large enough size. In our system, the reaction medium is much larger than the spiral wavelength (aspect ratio ≈ 50). Therefore, from our experimental results, the S−C boundary in the phase diagram is possibly the onset of the Eckhaus instability.

Due to the complexity of reaction network in our system, it is difficult to deduce the important values of α and β in eq 2. Thus, quantitative comparison between our experimental results and the theoretical analyses on CGLE cannot be fully made. Sørenson et al.[33] developed a good method, the quenching technique, to calculate these values from experimental data. In our experiment, however, since there are multiple concentration gradients across the reaction medium, we do not know the chemical compositions in the patterned layer. So their method cannot be applied in this experiment. Another possibility is to get these values from eq 3. If we know υ_g and q at the onset of the Eckhaus instability, we can deduce the values of α and β. In the experiment, although we can measure all the physical quantities of modulation and carrier waves, to get rescaled values, we need to know the characteristic time τ_0 and the correlation length ξ_0, which in turn depend on the chemical compositions of the system. Thus we have to settle for less quantitative results.

Our experimental results show that a local modulation saturates in time for a given control parameter; see Figure 6b,c. However, due to the finite reactor size, we do not know whether the amplitude of modulation can be saturated as a function of space or if it is just a long-lived transient. Janiaud et al.[31] analyzed the nonlinear behavior of phase modulation $\phi(x,t)$ near the onset of the Eckhaus instability. Their analysis indicates the existence of stable compression pulses in a certain domain of parameters near the onset of the Eckhaus instability. These pulses are possibly transient for the experimental parameters. Our experiments in the finite reaction medium have shown a similar result.

The generation of defects that we consider is induced by the local wavelength being below the minimum value allowed by the dispersion relation. However, our data show that, within the experimental uncertainty, the amplitude of phase modulation is *not* increasing along the distance from the center even beyond the onset of the instability (see Figure 5d). Therefore, why the generation of defects always takes place in a defined distance from the spiral center is still unraveled.

The observation of two behaviors of modulation waves hints that the major source of perturbations may be different in different regimes. We postulate that near the onset of the Eckhaus instability, perturbations mainly originate from the spiral tip. Because of the linear instability, the perturbations are quickly amplified as the spiral waves travels downstream and then saturated by the nonlinear effects. When the system is far beyond the Eckhaus instability, the amplitude of perturbations becomes very large. These perturbations may in turn influence the movement of spiral tips. A more satisfactory theoretical explanation has to be developed.

Acknowledgment. We thank H. L. Swinney for providing us with porous glass disks. This work is supported by the Chinese Natural Science Foundation.

References and Notes

(1) Dadivenko, J. M.; Pertsov, A. V.; Salomonsz, R.; Baxter, W.; Jalife, J. *Nature* **1992**, *355*, 349.

(2) Winfree, A. T. *Science* **1994**, *266*, 1003.
(3) Witkowski, F. X.; et al. *Nature* **1998**, *392*, 78.
(4) Coullet, P.; Gil, L.; Lega, J. *Phys. Rev. Lett.* **1989**, *62*, 1619.
(5) Eckmann, J.-P.; Procaccia, I. *Phys. Rev. Lett.* **1991**, *66*, 891.
(6) Hub, G.; Alstrøm, P.; Bohr, T. *Phys. Rev. Lett.* **1992**, *69*, 2380.
(7) Aranson, I.; Kramer, L.; Weber, A. *Phys. Rev. Lett.* **1994**, *72*, 2316.
(8) Ipsen, M.; Sørensen, P. G. *Phys. Rev. Lett.* **2000**, *84*, 2389.
(9) Ouyang, Q.; Flesselles, J. M. *Nature* **1996**, *379*, 143.
(10) Belmonte, A.; Flesselles, J.-M.; Ouyang, Q. *Europhys. Lett.* **1996**, *35*, 665.
(11) Park, J.-S.; Lee, K. J. *Phys. Rev. Lett.* **1999**, *83*, 5393.
(12) Ouyang, Q.; Swinney, H. L.; Li, G. *Phys. Rev. Lett.* **2000**, *84*, 1047.
(13) Bär, M.; Hildebrand, M.; Eiswirth, M.; Falcke, M.; Engel, H.; Neufeld, M. *Chaos* **1994**, *4*, 499.
(14) Bär, M.; Or-Guil, M. *Phys. Rev. Lett.* **1999**, *82*, 1160.
(15) Goryachev, A.; Chaté, H.; Kapral, R. *Phys. Rev. Lett.* **1998**, *80*, 873.
(16) Goryachev, A.; Chaté, H.; Kapral, R. *Phys. Rev. Lett.* **1999**, *83*, 1878.
(17) Kneener, J. P.; Tyson, J. J. *Physica* **1986**, *D21*, 307.
(18) Dockey, J. D.; Kneener, J. P.; Tyson, J. J. *Physica* **1988**, *D30*, 177.
(19) Barkley, D. *Phys. Rev. Lett.* **1994**, *72*, 164.
(20) Lázár, A.; Noszticzius, Z.; Farkas, H. *Chaos* **1995**, *5* (2), 443.
(21) Hakim, V.; Karma, A. *Phys. Rev. E* **1999**, *60*, 5073.
(22) Zhou, L. Q.; Ouyang, Q. *Phys. Rev. Lett.* **2000**, *85*, 1650.
(23) Karma, A. *Nature* **1996**, *379*, 118.
(24) Ouyang, Q.; Swinney, H. L. *Chaos* **1991**, *1*, 411.
(25) Pearson, J.; Bruno, W. *Chaos* **1992**, *2*, 513.
(26) Duffiet, V.; Boissonade, J. *Phys. Rev. E* **1996**, *53*, 4883.
(27) Ouyang, Q.; Li, R.; Li, G.; Swinney, H. L. *J. Chem. Phys.* **1995**, *102*, 2551.
(28) Li, G.; Ouyang, Q.; Petrov, V.; Swinney, H. L. *Phys. Rev. Lett.* **1996**, *77*, 2105.
(29) Belmonte, A. L.; Ouyang, Q.; Flesselles, J. M. *J. Phys. II Fr.* **1997**, *7*, 1425.
(30) Note: One can recover the linear equation satisfied by the perturbation $\phi(x,t)$ (or $a(x,t)$) from the dispersion relation (eq 3 in the text): $\partial p/\partial t = v_g(\partial\phi/\partial x) + D_{||}(\partial^2\phi/\partial x^2)$. The first term on the right is the convection term whose velocity is v_g, and the second term represents the diffusion. Thus, we say that the long wavelength instability has a convective nature.
(31) Janiaud, B.; et al. *Physica* **1992**, *D55*, 269.
(32) Aranson, I. S.; Aranson, L.; Kramer, L.; Weber, A. *Phys. Rev. A* **1992**, *46*, R2992.
(33) Kramer, L.; Hynne, F.; Sørenson, P. G.; Walgraef, D. *Chaos* **1994**, *4*, 443.